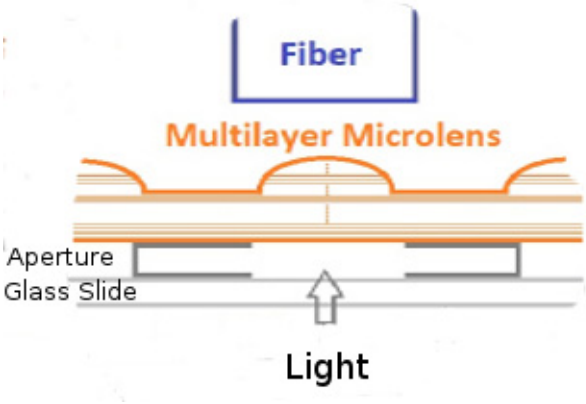

Fig. 2. Experimental setup for characterizing the spectral dispersion of the focusing properties of the microlenses.

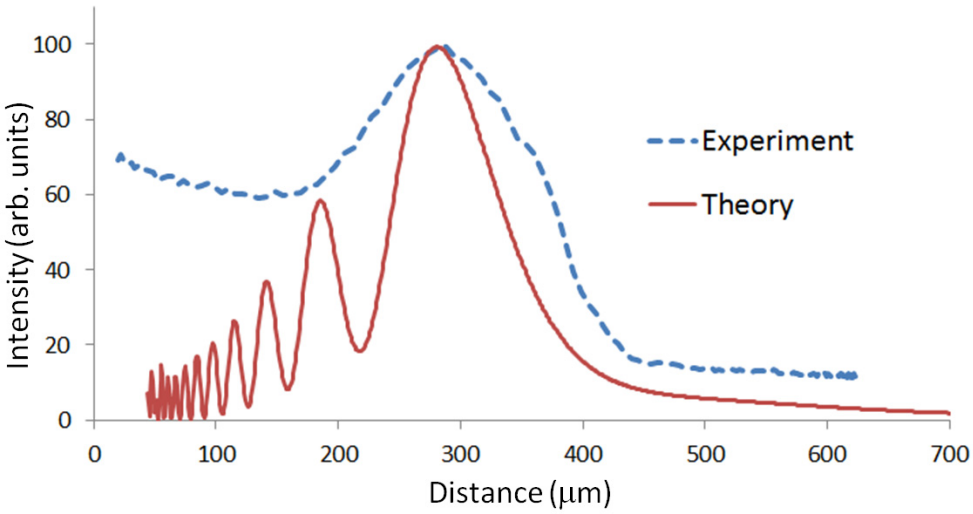

Fig. 3. The dashed blue trace is a typical multilayered co-extruded polymer microlens light curve of captured focused light. The wavelength for this light curve is 695±.5 nm and the focal length is ∼ 300 microns. The solid red trace is an idealized light curve, from physical optics theory assuming monochromatic light (∼ 695 nm) incident along the optical axis of the microlens whose dimensions are given in Section 4.

"light curve") for each wavelength. A representative measured light curve (dashed blue trace) at a single wavelength is shown in Fig. 3 along with a typical theory curve (solid red trace). The location of the peak indicates the approximate focal length. The qualitative difference between the theory and experiment is primarily a consequence of the non-ideality of the lens and underlying multilayer structure as well as the geometry/acceptance of the fiber. The calibration of the distances in the actuating stage is accomplished with a micrometer, yielding a distance versus current calibration that is accurate to about 10% in determining the absolute focal length, but can fix the dispersion much more precisely.

In addition, the focused beam waist was measured under white light using a NIKON Eclipse

#217124 - $15.00 USD Received 16 Jul 2014; revised 1 Nov 2014; accepted 3 Nov 2014; published 19 Nov 2014

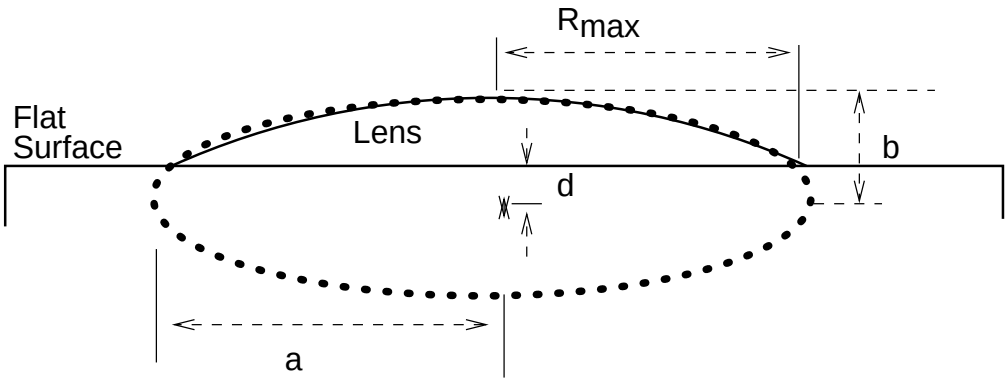

Fig. 4. Fixing the notation for a section of an oblate spheroid lens, showing ellipse semimajor (a) and semiminor (b) axes, the outer radius of the raised plano-convex lens shape R_{max}, and the depth of the center of the ellipse (d) below the plane of the surface supporting the lens.

M600 microscope (objective 100×/0.9) to determine the spot size on a 1.3 MPixels CMOS array and found to be $3.3 \pm 0.5 \mu m$, which is close to the approximate expected diffraction limit of the microlens ($\sim 3\mu m$).

4. Theory and data analysis

To model the dispersive optical properties of the multilayered microlens, rather than full Finite-Difference Time-Domain (FDTD) simulation, we use Huygen's principle and add up the spherical waves coming from each section of the lens, while paying careful attention to the phase retardation at each surface due to the wave's propagation through the layered microlens [29].

Refer to Fig. 4 to fix the geometrical parameters we use to describe the lenses (*i.e.* as a section of an oblate spheroid formed by rotating an ellipse about its minor axis). In terms of these parameters, the radius of curvature at the center of the lens is $\tilde{R} \sim \frac{a^2}{b}$, and so, were it a monolithic lens of material index n, the thin lens approximate focal distance would be $f \sim \frac{a^2}{(b-d)(n-1)}$. Note that $R_{max} = a\sqrt{1-\frac{d^2}{b^2}}$, in terms of which

$$\tilde{R} = \frac{R_{max}^2}{b-d}\frac{b}{b+d}, \tag{1}$$

an expression that smoothly interpolates between the elliptical and parabolic cross-section limits, in which $\tilde{R} = \frac{R_{max}^2}{2h}$ and $f = \frac{\tilde{R}}{(n-1)}$ and altitude $h = b - d$. By altitude we are referring to the maximum height of the microlens surface above the flat segment between lenses.

Because we are most interested in the far-field, we simply add up spherical waves

$$\mathrm{d}\psi = z_h \frac{e^{ik_0 r}}{r}\mathrm{d}A \tag{2}$$

emanating from each surface dA of the ring of height h making up the lens, with z_h being the magnitude and phase of the wave as it emerges from that surface (r is the distance to the point at which we are combining all of the waves) and where k_0 is the magnitude of the vacuum wavevector. Technically, the integration must include all of the illuminated surfaces, including the flat parts, but in the case of uniform illumination we can use linearity to reduce it to just an integral across the lens.

#217124 - $15.00 USD Received 16 Jul 2014; revised 1 Nov 2014; accepted 3 Nov 2014; published 19 Nov 2014

The final simplification we employ comes from the paraxial limit. In general, the computation of the far fields can be written as sums of elliptics or (in the case of azimuthal symmetry) Bessel functions [29]. In the paraxial limit, a distance $X >> 2R_{max}$, but much closer to the optical axis than $X\lambda/R_{max}$, the integrations simplify and can be written in terms of exponentials. On axis, each annular section (of r_{outer} outer and r_{inner} inner radius) at height h of the lens contributes to the wave sum an amplitude S_h given by

$$S_h = \frac{1}{X-h}\int_{r_{inner}}^{r_{outer}} r dr e^{i\frac{k_0 r^2}{2(X-h)}}(z_h e^{-ik_0 h}-1), \tag{3}$$

where we have removed an irrelevant overall phase factor and have taken the difference between the amplitude and phase of the wave emerging from that height of material and that amplitude (unity) and phase ($e^{ik_0 h}$) that would have emerged from there *were there no lens there at all*.

Thus, for each annulus that makes up the lens, the contribution it makes to the on-axis far field (at position X) is

$$S_h = \mathscr{A}(z_h e^{-ik_0 h}-1)[e^{i\frac{k_0 r_{outer}^2}{2(X-h)}} - e^{i\frac{k_0 r_{inner}^2}{2(X-h)}}], \tag{4}$$

where $\mathscr{A}$ is some overall amplitude which scales with the input wave's amplitude and is the same for all annuli. Thus, the total wave amplitude S at a distance X from the lens but on axis is $S_{tot} = \sum_h S_h$. These expressions are complicated to evaluate for layered materials because z_h is an intricate function of h. For the well known case of a monolithic plano-convex lens, however, one can compute this sum analytically, recovering in the thin lens limit the familiar results of a Gaussian beam focal distance and waist.

To find z_h rigorously would require that one solve Maxwell's equations for the wave field in this layered geometry, or obtain it numerically via a finite element (for example, via FDTD) simulation. More intuitively, we adopt an approximate z_h, namely, we estimate z_h from the transmission amplitude for this normal incident wave to exit a stack of these multilayers that would have terminated at h. Physically this approximation includes only internal reflections in the full multilayer from the layers below height h, discounting reflections from the rest of the lens that contribute to the wave emanating from the annulus at height h.

The modulus square of the resulting S_{tot} as a function of X, the distance along the axis, typically leads to a light curve as in Fig. 3 (red solid trace) as compared with the measured light curve (blue dashed trace) for one of the layered microlenses. Note that the theory trace can be thought of as plot of the intensity (essentially, $|S_{tot}|^2$) on the lens axis versus distance (X) from the lens. We identify the maximum of this light curve as the focal length of the lens at this wavelength, and note that at large X, ignoring background light, the intensity falls off universally as $1/X^2$, as expected. In experiment, the interference fringes at intermediate X are generally smeared out due to spectral and spatial averaging.

Equating the location of the on-axis light curve maximum with the focal length, theory indicates that these lenses will typically have large, designable chromatic aberration. The solid green trace of Fig. 5 is a typical theoretical curve depicting $\delta f/f$, the fractional variation in the focal distance with wavelength, for a microlens with (compare Fig. 1(d) and Fig. 4) $d = 0.27$ microns, $a = 34$ microns, $b = 2.5$ microns built from a 32-layer multilayer lens blank having a reflection band stretching from 430 nm to 510 nm (as shown in transmission curve (dashed red) of Fig. 5). In essentially all cases, the theory model predicts focal lengths for these multilayered convex lenses that are shorter on the red (long wavelength) side of the band edge than the blue side, opposite to the usual expectations of chromatic aberration in a solid lens of a material with normal dispersion. As described below, this shape can be understood in terms of the effects of the transmission band structure created by the multilayering (again, for example

#217124 - $15.00 USD Received 16 Jul 2014; revised 1 Nov 2014; accepted 3 Nov 2014; published 19 Nov 2014

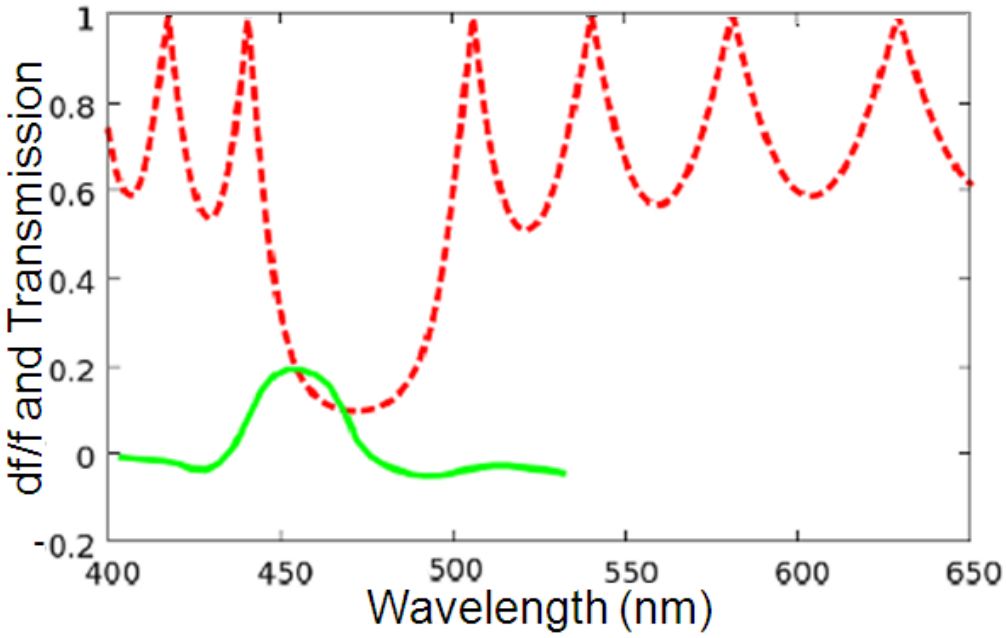

Fig. 5. Multilayered microlens computed focal length dispersion using physical optics theory described in the text. The dashed red trace is the computed transmission band of the 32 perfectly uniform layer model (layer indexes of 1.58 and 1.44) showing a reflection band between 440 and 510 nm. In solid green is the computed fractional change in the focal length (df/f) of the multilayer structure showing a profound change around the reflection band edge.

as shown by the dashed red trace in Fig. 5). FDTD calculations for a plano-convex shape in Fig. 4 reveal that there is little noticeable change in the focus spot size across the reflection band, and, further, that the spot size corresponds closely to that of a monolithic lens. As an additional check we note that these more detailed numerical calculations show the same qualitative changes in the focal length as the wavelength varies across the reflection band as are seen in the simple semi-analytical model described above (Fig. 5) and as noted in experiment (Fig. 6).

5. Discussion

Figure 6 shows the measured transmission band and focal length variations of a single multilayered PS/PMMA polymer microlens of radius $\sim 28\pm4$ microns and height about $2.5\pm.5$ microns. These measurements were made using AFM and the stated variations are due to process variations across the microlens array, not dimensional uncertainty in the measurements of a single lens. In that figure, the shallow reflection band stretching from 430 nm to 510 nm is easily discernable, as is the pronounced chromatic aberration in the focal distance of nearly 30 percent in a span of 25 nm. The measured average focal length was $\sim 300\pm20$ microns. Note that this is broadly consistent with expectations for a thin lens of material whose index is the average of the constituent polymer indices. The scatter in the focal lengths at each wavelength is technical noise associated with the jitter in the numerics associated with determining the maxima of each of the experimental light curves. Fitting the portion of that df/f versus λ curve away from the reflection band reveals the nominal changes in the focal length expected

#217124 - $15.00 USD Received 16 Jul 2014; revised 1 Nov 2014; accepted 3 Nov 2014; published 19 Nov 2014

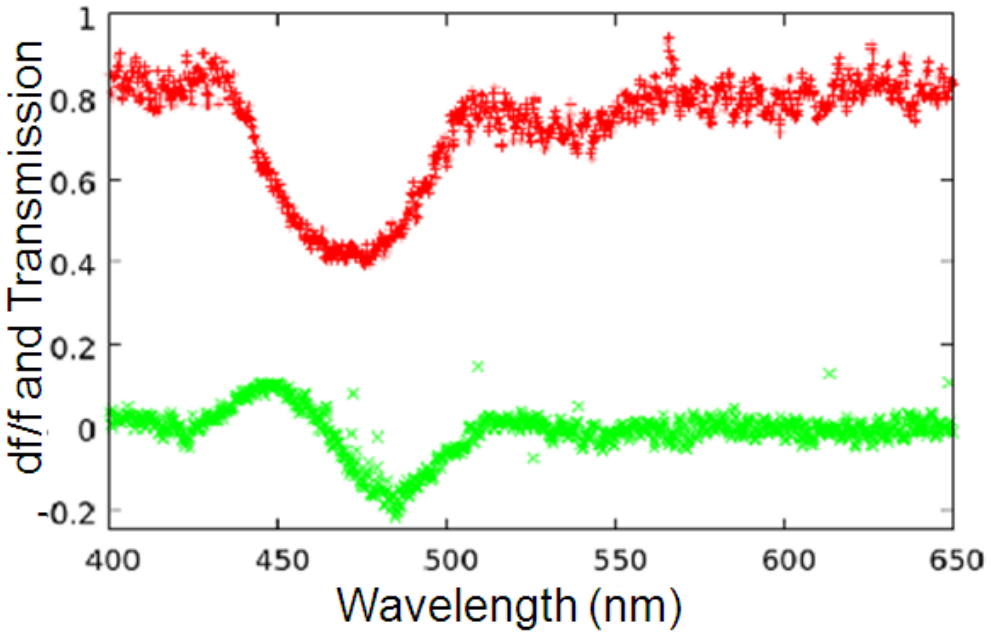

Fig. 6. Measured layered microlens focal length dispersion (green '$\times$') using the fiber transport system described in the text and the layered material's transmission spectrum (red '$+$'). The lens material has an easily discernable shallow reflection band from about 430 nm to 510 nm. The len's focal length dispersion is pronounced across the band, amounting to nearly 25% changes in the $\sim$300 μm focal length.

from dispersion in these bulk materials, albeit reduced somewhat from the diffractive effects from the smallness of the lens itself. For comparison, the expected (fractional, normal) chromatic aberration in a focal distance of a lens made from a (unlayered) PS/PMMA blend in this wavelength range (500-1000 microns) is expected to be roughly 2% per octave, and a linear fit in this wavelength range of our data is consistent with roughly 1% per octave. This and the regular shape of the light curves away from the material's reflection band (Fig. 3, blue dashed trace) further support the identification of this feature with a microlens of the shape imaged in Fig. 1.

The qualitative similarity between the experimentally measured focal length dispersion and that derived from the simple physical optics model can be readily understood in terms of where the light lingers as it flows through the material. Recall that for these binary multilayers, at the short wavelength edge of an optical band, the light's electric fields are primarily in the low index material whereas, at the long wavelength band edge, they reside primarily in the high index material. Thus, because the effective index that the light fields respond to at the long wavelength side is closer to the lower index material's, the focal length is larger, and vice versa. This simple narrative also leads to an estimate for the upper bound of the focal length variation; because the focal length is inversely proportional to $(n-1)$, we expect a change across the band of $(n_{high}-n_{low})/(\bar{n}-1) \sim 20\%$ (for a PS/PMMA layered film), akin to that measured. Further discussion of errors due to layer thickness variations and imperfections due to the photolithography etching process are beyond the scope of this demonstration [12, 31].

#217124 - $15.00 USD Received 16 Jul 2014; revised 1 Nov 2014; accepted 3 Nov 2014; published 19 Nov 2014

6. Conclusions and future work

We have created layered microlenses with designed chromatic aberration in the visible. A simple physical optics model for the transmission and focusing of the light traversing these microlenses shows how the 'structural' dispersion caused by the layering leads to this designed chromatism. Even though such chromatism occurs in the multilayer material's reflection band, the number and properties of the layers can be designed and tuned to still allow a substantial percentage of the light through, while preserving the chromatism. We have studied these microlens structures primarily as a test of our overall understanding of the role of designed dispersion in layered microlenses, with potential applications in multi-spectral imaging, and dispersion correction and control.

Our work here builds upon earlier work demonstrating the benefits of a roll-to-roll coextrusion process for multilayering to create Bragg reflectors [27, 30] and distributed feedback lasers [23, 25, 32]. We emphasize that the simple multilayer stack design used is not necessarily ideal for applications and we did not investigate these materials for imaging applications, but we have used this system to better understand the feasibility of the novel combination of an axially-cut, lens-like pattern in a multilayer polymer.

Beyond the polymer combinations used here, this work connects the designed optical dispersion in metamaterials in the visible with the properties of a lens. Depending upon the parameters of the etching process, the resulting shape may be smoothly varying through the layers or can be etched in a terraced layer-cake structure by taking advantage of different etching speeds in the different polymers. In an effort to understand more fully the connection between multilayer design and the chromatic properties of the lens, we are currently trying to make multilayered lenses with higher numerical aperture as well as exploring novel polymer multilayer optical materials such as those with designed phase-slip defects formerly used in laser and magneto-optics studies [30, 32]. Optical transport in these phase-slip defect multilayers is well understood and will make lenses ideal for more rigorous testing of our model. Because we can also create multi-band, gradient, and 'chirped' structures as described in [33], we are exploring the utility of lenses made from materials with more intricate customizable dispersion. For future development, we note that a grayscale mask can be used with multilayers to create a circular grating structure that has been shown to be an attractive structure for confining modes in a surface-emitting photonic bandgap laser [34]. Combining the surface structuring with the multilayer Bragg structure is one approach to a more easily fabricated three-dimensional photonic crystal.

Acknowledgments

The authors are grateful to the National Science Foundation for financial support from the Science and Technology Center for Layered Polymeric Systems under grant number No. DMR 0423914 and separately under grant number ECCS-1360725 and also grant DMR 1229129. We also acknowledge support from the State of Ohio, Department of Development, State of Ohio, Chancellor of the Board of Regents and Third Frontier Commission, which provided funding in support of the Research Cluster on Surfaces in Advanced Materials.

#217124 - $15.00 USD Received 16 Jul 2014; revised 1 Nov 2014; accepted 3 Nov 2014; published 19 Nov 2014